

# Design and Characterization of plastic scintillating detectors for next-generation neutrino experiments

Santiago Brunner

Supervisor: Davide Sgalaberna

Co-supervisor: Matthew Franks

June 2024

## Abstract

Scintillating materials are essential for detecting neutral particles, such as neutrinos. They emit detectable photons, when traversed by energetic particles. This study explores the effects of different resins on the photon detection efficiency of plastic scintillating fibers, which are crucial for tracking particles in neutrino detectors like ND280 of the T2K experiment. We compared three types of resins: UV-sensitive resin from Anycubic (AC), EJ-500 optical cement (EJ), and OF-133-V3 (OF), with respective refractive indices of 1.52, 1.57, and 1.33. Our experimental setup included measuring the number of photons detected per event for short (12 cm) and long (2 m) fibers before and after applying the resins. The results for both fibers indicated that the OF resin, with the lowest refractive index, had the least impact on photon loss. On average along the 2m-fiber, it captured  $(97.1 \pm 6.5)\%$  of the emitted photons, while for the short fiber it was  $(89.8 \pm 3.6)\%$ . Contrary to expectations, the EJ resin performed better than the AC resin for the long fibers, despite its higher refractive index. On average EJ and AC captured  $(86.0 \pm 9.8)\%$  and  $(60.1 \pm 10.5)\%$  of the emitted photons, respectively. There was no significant difference between EJ and AC for the short fibers. The study provides valuable insights into the choice of resin for minimizing photon loss in scintillating fibers, with OF resin being the most suitable for high-resolution neutrino detectors. Future work will focus on the long-term effects of these resins on the fibers' performance.

# Contents

<b>1</b>	<b>Introduction</b>	<b>3</b>
1.1	Scintillating Fibers . . . . .	4
1.2	Readout System . . . . .	6
<b>2</b>	<b>Experiment</b>	<b>7</b>
2.1	Sample Preparation . . . . .	7
2.2	Application of resin . . . . .	8
2.3	Measurements of the short samples . . . . .	9
2.4	Measurements of the long fibers . . . . .	10
<b>3</b>	<b>Data analysis</b>	<b>12</b>
3.1	Determination of the Gain . . . . .	12
3.2	Determination of the Most Probable Value . . . . .	12
<b>4</b>	<b>Results</b>	<b>14</b>
4.1	Short Fibers . . . . .	14
4.1.1	Error analysis . . . . .	14
4.2	Long Fibers . . . . .	14
4.2.1	Error Analysis . . . . .	15
<b>5</b>	<b>Discussion</b>	<b>17</b>
<b>6</b>	<b>Conclusion</b>	<b>18</b>

# 1 Introduction

Neutrinos are elementary particles with extremely small masses and no electric charge, making them one of the most elusive particles. They are produced in various nuclear reactions, such as those in the Sun, nuclear reactors, and during supernovae. It has been shown that the violation of the CP symmetry in leptons, such as neutrinos, could be the reason for the matter-antimatter asymmetry in the universe [1]. This CP violation can be detected by investigating muon neutrino to electron neutrino oscillations.

In the T2K (Tokai to Kamioka) [2] experiment, a pure muon (anti-) neutrino beam is produced at the accelerator complex J-PARC at the east coast of Japan and is detected at two different detectors: the near detector complex placed 280 m from the source and the far detector, called Super Kamiokande (SK), which consists of a water Cerenkov detector placed at a distance of 295 km, see Fig. 1. At this distance, the probability for an oscillation from the muon to the electron neutrino is the highest.

The near detector is used to characterize the neutrino beam before any oscillations occur, while the far detector measures the beam after it has travelled a long distance and has probably undergone oscillation.

The near detector consists of the on-axis detector INGRID [3] and the off-axis detector ND280 [4], the upgraded version of which is illustrated in Fig. 2. One important part of the latter is the SuperFGD, which serves as an active neutrino target. It consists of independent  $1 \times 1 \times 1$  cm $^3$  cubes that allow to track the path of protons with a momentum of 220 MeV/c [5]. To resolve shorter paths of protons with lower momentum, we need a finer detector. This could be achieved with 1mm  $\times$  1mm scintillating fibers.

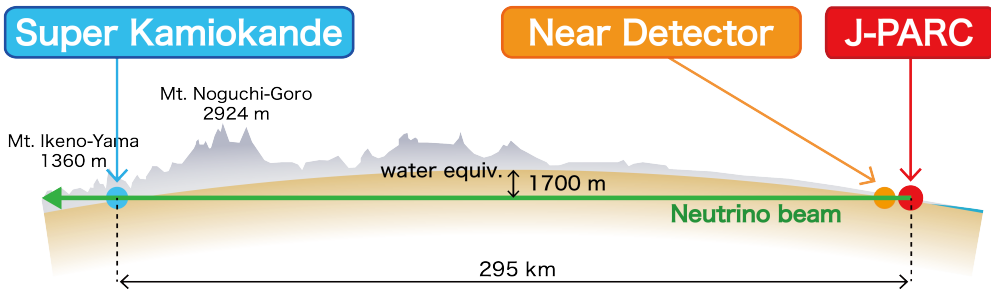


Figure 1: Schematic view of the T2K experiment configuration. At the near detector location, there are two detectors: one is the off-axis near detector ND280 and the other is the INGRID on-axis near detector (Source: [6]).

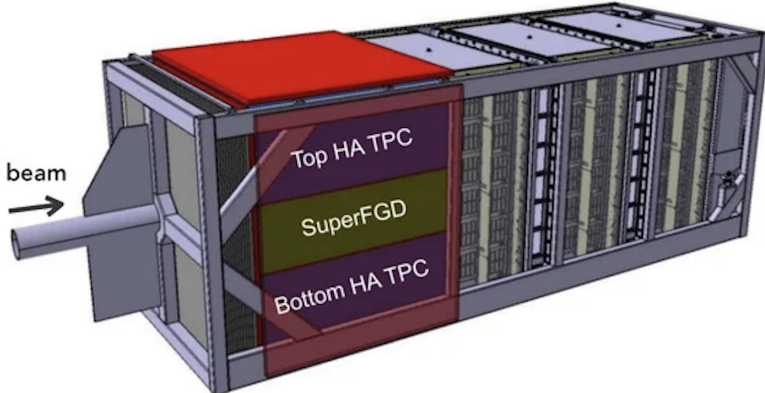


Figure 2: Picture of the upgraded near detector ND280 (Source: [7]).

Scintillating materials are commonly used to detect neutral particles like neutrinos [8]. They can be used as active volume in neutrino detectors such as in the near detector ND280. As the particles traverse the scintillating material they transfer their energy to the material which in turn emits that energy in form of photons. Using photosensors, we are able to detect those photons. By grouping multiple layers of scintillating fibers, it is possible to reconstruct and track the path of the particles in three dimensions within the active volume [9]. In that study, the active volume consists of multiple loose fibers. Depending on the size of the detector, an enormous amount of single fibers would be needed. Such an amount is very difficult to keep under control, even more so, if the diameter of the fibers is to be decreased in order to improve the resolution and therefore be able to track paths of sub-mm length. For future upgrades of ND280 the fibers must be locked in place. One possibility to do so, is to glue the fibers together using EJ-500 epoxy cement [10] like in [11]. This kind of resin has the disadvantage of taking several days to cure completely, which is why we will consider other kinds, such as UV sensitive resins.

## 1.1 Scintillating Fibers

In this project, we are investigating the effects of different resins on scintillating fibers. These fibers work as waveguides, as they confine light rays with sufficiently small angles with respect to the planar interface of the core and the cladding. The light bounces back and forth as it propagates along the fiber until it reaches our detector as sketched in Fig. 3. We can calculate the critical angle  $\theta_c$  for total internal reflection for a general interface between

media of refractive indices  $n_1$  and  $n_2$  with the formula

$$\theta_c = \cos^{-1}(n_2/n_1). \quad (1)$$

Considering that there can also be reflection at the cladding-air interface, we can calculate the maximal angle  $\theta_{\max}$  at which the photon can be emitted to be confined inside the fiber using Snell's law. We used squared fibers from the company Kuraray with refractive indices of  $n_{\text{core}} = 1.59$  and  $n_{\text{clad}} = 1.49$ , respectively [12]. We find  $\theta_{\max} = 46.0^\circ$ . Light with a larger angle will be transmitted through the surfaces and therefore be lost.

When resin is applied,  $\theta_c$  gets smaller, since usually  $n_{\text{resin}} > n_{\text{air}}$ . Consequently,  $\theta_{\max}$  gets smaller as well, the actual value depending on  $n_{\text{resin}}$ . The higher the refractive index of the resin, the smaller  $\theta_{\max}$ , so that less photons can be detected. In Fig. 3 different scenarios are depicted for the cases where no resin is applied,  $n_{\text{resin}} < n_{\text{clad}}$  and  $n_{\text{resin}} > n_{\text{clad}}$ . In Fig. 3b, the photons can still be reflected, but  $\theta_c$  is much smaller than in Fig. 3a. Differently in Fig. 3c, where light cannot be reflected at all, as can also be seen from equation (1), where there is no solution for  $\theta_c$ .

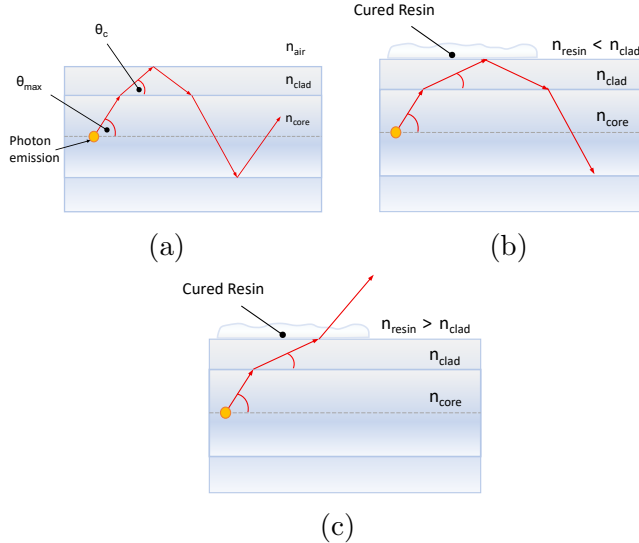


Figure 3: Path (red) of the light generated inside the scintillating fiber for three different cases: (a) No resin applied, (b)  $n_{\text{resin}} < n_{\text{clad}}$  and (c)  $n_{\text{resin}} > n_{\text{clad}}$ . Notice that the angle  $\theta_c$  in (b) is much smaller than in (a), since  $n_{\text{resin}} > n_{\text{air}}$ .

## 1.2 Readout System

We use a Multi-Pixel Photon Counter (MPPC), also called Silicon Photomultiplier (SiPM) from Hamamatsu [13] placed at one end of each fiber to count the photons propagating along the fiber. A SiPM is a solid state device consisting of a matrix of pixels that can detect these photons with high sensitivity, converting each photon event into a corresponding electrical pulse [14].

These pulses are then processed by the CAEN DT5202 [15], which uses a pre-amplifier to enhance the signal strength. Afterwards, these signals are digitized by an analog-to-digital converter (ADC), which quantifies the height of the pulse with the number of photons.

Finally, we obtain from the software called Janus [16] a histogram counting the number of events that led to a certain ADC value. The ADC value can be transformed into number of photons with the following formula:

$$\text{number of } \gamma = \frac{\text{ADC} - \text{Pedestal}}{\text{Gain}}, \quad (2)$$

where the pedestal defines “the position of the pulse height converted values, when no signal is present” [16]. The actual value for the gain can be determined by fitting Gaussian curves to the histogram. This will be explained in more detail in section 3.1.

## 2 Experiment

The aim of this experiment is to analyse the effects different types of resins have on detectors using plastic scintillating fibers, commonly used to detect neutral particles such as neutrinos. An important aspect will be the loss of light the resins generate. We are comparing three different resins: the UV sensitive resin from Anycubic (AC) [17], EJ-500 optical cement (EJ) [10] and OF-133-V3 (OF) [18]. The refractive indices are as follows:  $n_{\text{AC}} = 1.52$ ,  $n_{\text{EJ}} = 1.57$ ,  $n_{\text{OF}} = 1.33$ . To simulate the neutrinos traversing the fiber, we will use beta particles radiated by a radioactive source of  ${}^{90}\text{Sr}$ . In the first part we will measure the number of photons detected per event, i.e. per charged particle going through the fiber, for four short fibers of  $12.0 \pm 0.5$  cm length. One for each type of resin and another one for comparison without resin, which we will abbreviate with NR for “no resin”. Additionally, we will measure the same quantity for three 2 m long fibers to see how the number of detected photons behaves with increasing distance between the source and the detector.

### 2.1 Sample Preparation

To be able to couple the scintillating fibers to the SiPM, we used a 3D printed connector, a scheme of which can be found in Fig. 4. It consists of a male part, where the fiber is glued to and a female part where the SiPM is placed.

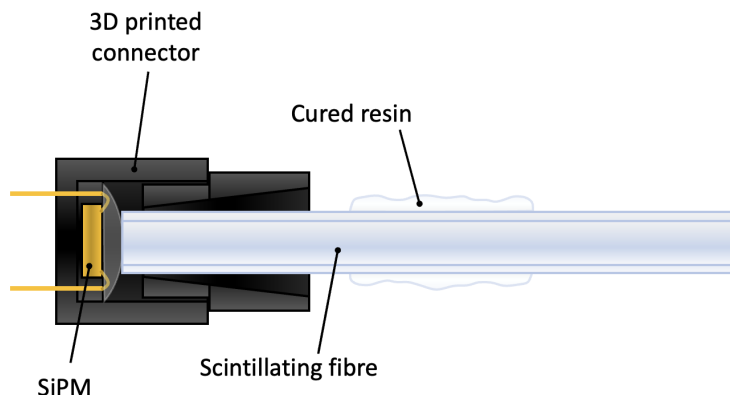


Figure 4: Scheme of the scintillating fiber coupling to the SiPM using the 3D printed connector.

Next, we needed to polish both ends of the fibers with sandpaper of different grit sizes. The reason for that is to have highly transmitting surfaces,

such that on one end of the fiber the photons can reach the detector easily, while on the other end the photons can be purposely lost instead of being reflected and falsely count by the detector on the other side. We used first a 800 grit sandpaper from 3M [19], followed by polishing sheets from Thorlabs with grit sizes of  $30\ \mu\text{m}$  and then  $3\ \mu\text{m}$  [20].

## 2.2 Application of resin

One important aspect of this project was to ensure reproducibility. For that, we looked for a controlled method to apply resin to the fibers. We created a mould out of silicone. The process can be found in Fig. 5: We 3D printed a cylinder with a diameter of 3 mm and a height of 5 cm with fiber-like cuboids on the top and bottom simulating the fiber. The whole 3D printed structure was placed inside a wooden box (Fig. 5a). The blue silicone was then poured into the wooden box (Fig. 5b). When the silicone was cured, we could remove the wooden box and cut through the surface of the cube to get the black cylinder out, leaving a cavity inside, where the fiber could be placed (Fig. 5c). Through that cut, we could pour the resin into the cylindrical cavity. Since the cavity was just below the surface, it was also possible to cure UV sensitive resin, such that the same type of mould could be used for all types of resins considered in this experiment. The applied resin on the fibers can be seen in Fig. 6. Using this mould resulted in a 6 cm long section of resin on the fiber.

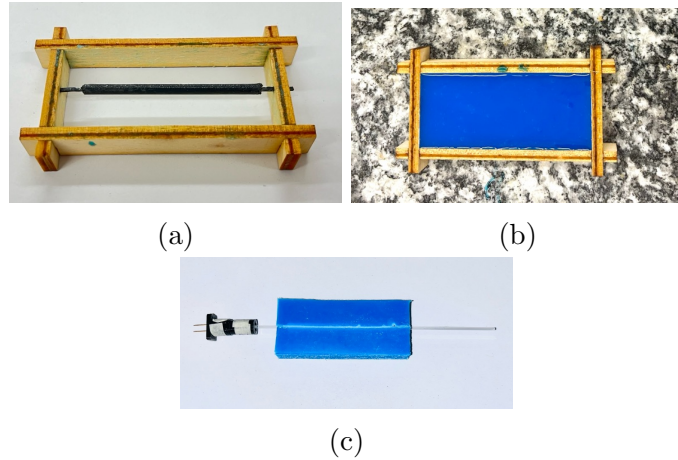


Figure 5: Process of creating a mould: (a) The 3D printed cylinder is placed in the wooden box. (b) The blue silicone is poured into it until it is cured. (c) The fiber can be placed inside the mould to apply the resin.



Figure 6: The four short fibers OF, EJ, AC, NR (from top to bottom) with the applied resin.

### 2.3 Measurements of the short samples

As already mentioned, we measured the number of photons created per event for four fibers. Three of which will have resin applied, while the forth one will be used for comparison. We measured the fibers before and after applying the resin to find how much light was lost due to the resin. The experimental setup can be found in Fig. 7 and was placed inside a dark box such that other sources of photons could be eliminated.

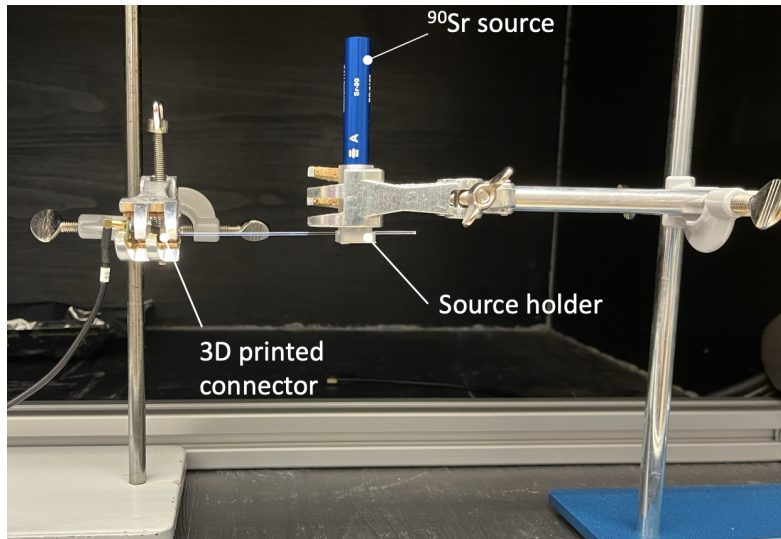


Figure 7: Setup used to measure the short fibers.

The readout system measured the incoming photons for 120 seconds. This

is considered one measurement. To minimize statistical errors and account for any fluctuations, we performed for each fiber five such measurements before and another five after applying the resin. After each measurement the fiber was changed, such that the process of setting up was also accounted for. The source was placed at a constant distance of  $(9.5 \pm 0.3)$  cm from the SiPM, where the error comes from setting the experiment up by hand.

## 2.4 Measurements of the long fibers

To measure the long fibers, a different setup was needed, since the fibers did not fit into the dark box without bending. We 3D printed “holders” with two rails where the fiber could be kept in place. These holders are depicted in Fig. 8. Additionally, we printed a source holder, which can keep the fiber on one rail in place while allowing the radioactive source to irradiate the fiber in the other rail. As can be seen, there is foam inside the rails, as well as on the lid, to prevent the plastic of damaging the cladding.

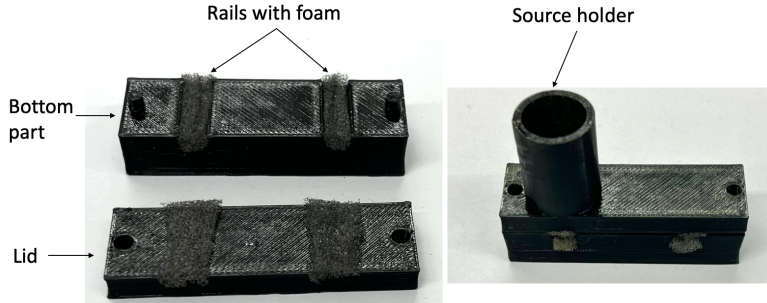


Figure 8: 3D printed holder to keep the fiber in place (left) and the additional source holder (right).

We arranged the fiber in a circular form as shown in Fig. 9, where the bending diameter was always greater than 30 cm to make sure there are no bending losses. (According to [12] the minimal bending diameter without losses is 20 cm.) The holders also made sure that the fiber did not touch the ground or itself.

We performed 20 measurements for three different fibers - one for each kind of resin - before applying the resin. With each measurement, we varied the distance between radiation source and detector. The source was placed at distances of  $(3.5 + k \cdot 10) \pm 0.5$  cm, for  $k \in \{0, 1, \dots, 19\}$ , from the SiPM. The error comes from the fact that the distance had to be measured by hand. Finally, we applied 19 segments of resin across the whole fiber, as described in

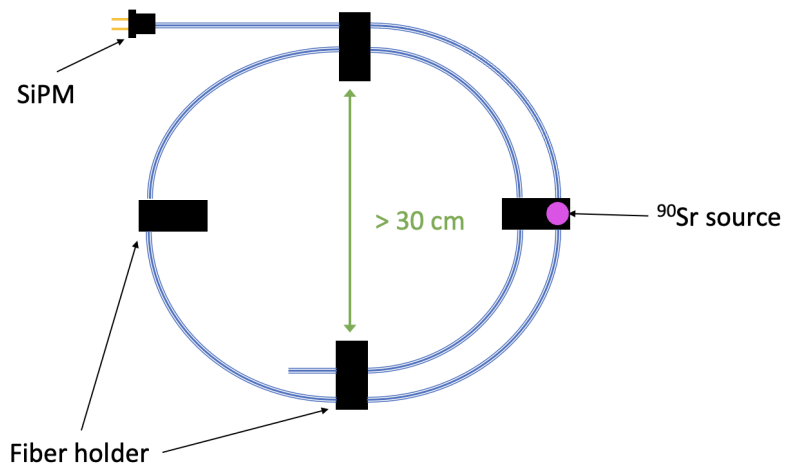


Figure 9: Schematic setup up to measure the long fibers.

section 2.2, leaving spacings of 4 cm between each segment where the source was placed and performed the same measurements at the same distances.

### 3 Data analysis

From the readout system, we obtained a histogram for each measurement that counted the times that the SiPM registered a certain ADC value, which can be converted to number of photons per event. We used the software ROOT to analyse the data.

#### 3.1 Determination of the Gain

From equation (2), we see that we needed to find the actual value for the gain. On the left side of Fig. 10 an example of a histogram is depicted, with a close up picture on the right, where sub-peaks can be seen. These appear because the digital value obtained for a certain amount of detected photons varies slightly because of external effects, leading to a Gaussian distribution.

The gain can be obtained from the distances between the peaks of the sub-peaks. We fitted Gaussian curves to the peaks such that the distance between them - and therefore the gain - could be determined.

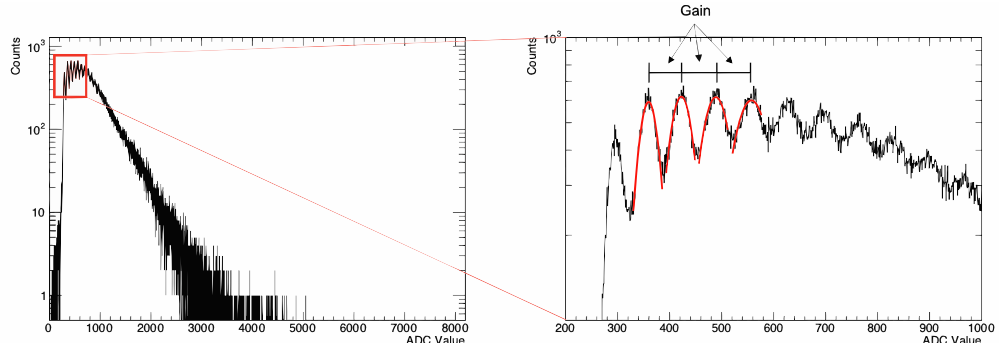


Figure 10: Example of a histogram of one measurement (left) with a closed up picture to visualize the oscillations (right).

#### 3.2 Determination of the Most Probable Value

To obtain the most probable value (MPV), we fitted a Gaussian curve to the whole histogram around the clear visible peak. To aid the fitting procedure, we increased the bin size of the histogram such that the curve was smoother. From the ADC value where the peak is located we can determine the most probable number of photons that are emitted for one event using equation (2) and a pedestal position of 50.

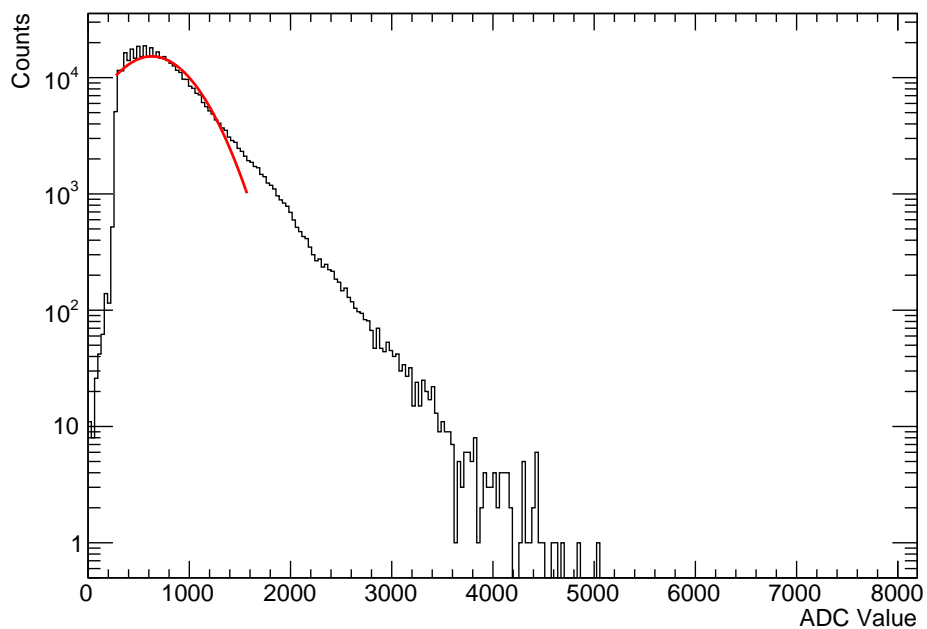


Figure 11: Example of a histogram with increased bin size to smoothen the curve, such that a Gaussian curve could be fitted.

## 4 Results

### 4.1 Short Fibers

To make up for any coupling differences between the fibers, we compared the photon count (PC) of the fibers after applying the resin, normalized with the PC before applying it. The results can be found in Fig. 12.

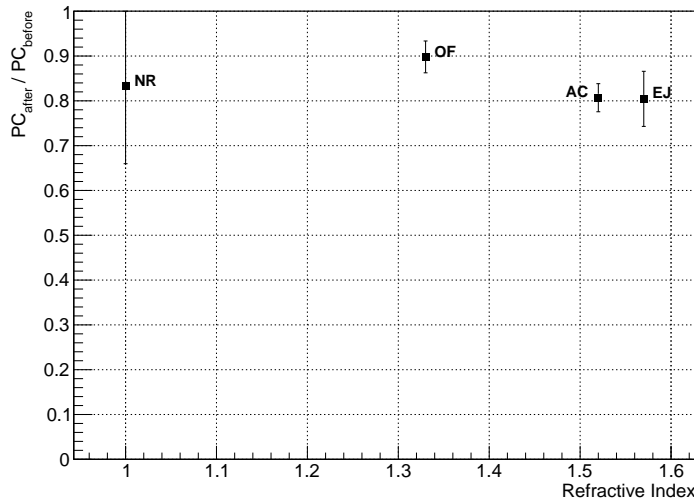


Figure 12: Comparison of the normalized photon counts for each kind of resin as a function of the corresponding index of refraction.

#### 4.1.1 Error analysis

We measured each fiber five times before and after applying the resin. From the standard deviations of the results for  $PC_{\text{before}}$  and  $PC_{\text{after}}$  we computed the error bars of Fig. 12 using Gaussian error propagation. Additionally, we assume no errors in the indices of refraction.

### 4.2 Long Fibers

We measured the PC of the three long fibers as a function of the distance between SiPM and the radioactive source. The results can be found in Fig. 13 and the average  $PC_{\text{after}}/PC_{\text{before}}$  along the fibers can be found in Tab. 1. We expected the PC of the measurements without resin to behave like a

double exponential curve and fitted the following model  $f(x)$  to our data:

$$f(x) = I_{\text{core}} \cdot e^{-\frac{x}{\lambda_{\text{core}}}} + I_{\text{clad}} \cdot e^{-\frac{x}{\lambda_{\text{clad}}}}, \quad (3)$$

where  $\lambda_{\text{core}}$  and  $\lambda_{\text{clad}}$  are the decay lengths for the core and cladding, respectively.

The fitting parameters are listed in Tab. 2.

[%]	AC	EJ	OF
$\text{PC}_{\text{after}}/\text{PC}_{\text{before}}$	$(60.1 \pm 10.5)$	$(86.0 \pm 9.8)$	$(97.1 \pm 6.5)$

Table 1: Average  $\text{PC}_{\text{after}}/\text{PC}_{\text{before}}$  along the whole fiber for the three resins.

Fiber	$I_{\text{core}}$	$\lambda_{\text{core}}$ [cm]	$I_{\text{clad}}$	$\lambda_{\text{clad}}$ [cm]
AC	$14.01 \pm 0.31$	$342.82 \pm 20.50$	$3.44 \pm 0.34$	$18.49 \pm 4.31$
EJ	$11.32 \pm 0.20$	$318.59 \pm 16.47$	$5.35 \pm 0.80$	$6.81 \pm 1.71$
OF	$10.46 \pm 0.18$	$400.00 \pm 94.58$	$3.66 \pm 0.46$	$24.60 \pm 9.48$

Table 2: Fitting parameters of the model given in (3) for the three long fibers.

#### 4.2.1 Error Analysis

Since we only could perform one set of measurements for each fiber, we could not estimate the error of the PC in Fig. 13 as we did for the short fibers in section 4.1.1 using the standard deviation of multiple measurements, which is why no error bars are plotted. The errors in the distance were estimated to be 1 cm because the source had to be placed by hand, but the corresponding error bars are too small to be seen in the plots.

The uncertainties in Tab. 2 were directly obtained from the fit function of the software ROOT.

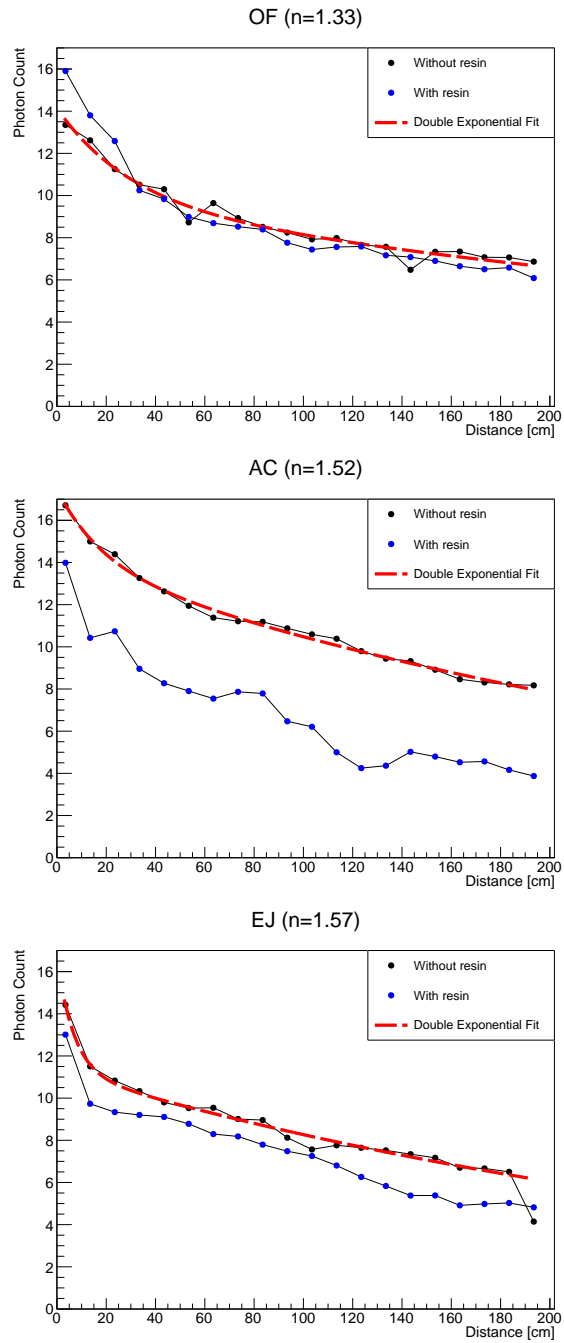


Figure 13: Results of the measurements of the long fibers OF, AC and EJ (from top to bottom): Photon count as a function of the distance between the SiPM and the source.

## 5 Discussion

In Fig. 12, we can see that the most expensive resin OF, which has the lowest refractive index, has the highest  $PC_{\text{after}}/PC_{\text{before}}$  value, meaning that it affects the photon detection the least, in accordance with our expectation. The AC and EJ resin have similar refractive indices as well as  $PC_{\text{after}}/PC_{\text{before}}$  values. Even though AC was expected to have a higher value than EJ, there is no significant difference between these resins, since the error bars overlap for this rather short distance of  $(9.5 \pm 0.3)$  cm to the SiPM.

Unfortunately, the NR fiber has very large error bars, making the result difficult to compare with the other fibers. Since we performed these measurements all within a couple hours and also changed the fiber after each measurement, environmental effects can be ruled out as a reason for the large uncertainty. One remaining reason might be a misalignment happening during the measurements in the coupling mechanism between fiber and SiPM.

The first thing to notice in Fig. 13 is that our simplified model in equation (3) adequately captures the observed data for all three data sets. For the lowest refractive index (OF), we find a very similar result to the short fiber measurements: This resin does not affect the attenuation length significantly, as can be seen from the fact that the data before and after resin coincide very well.

We would expect the area between the data points with (blue) and without (black) resin to grow, the greater the refractive index. This is not the case. Comparing the AC and EJ resin, we find that AC affects the PC much more than EJ for all distances, in contradiction to our expectations. Here, environmental changes can indeed be a reason. Since the measurements were much more time consuming than for the short fibers, we could not perform all measurements on the same day. Even though the dark box should always be completely dark, there might have been slight fluctuations on the different days. Additionally, any temperature difference might affect the performance of the SiPM. Although the last point should not be the main reason for the unexpected difference between AC and EJ, it is an important point we must not neglect.

## 6 Conclusion

In this project, we were able to setup a repeatable experiment to examine the effect of three kinds of resins with different refractive indices on plastic scintillating fibers and their ability to guide photons. From our results, we can conclude that the resin with the lowest refractive index (OF) indeed performed the best, barely influencing the PC. The results of the other two resins were not as expected, as the one with the highest refractive index (EJ) lost less photons, after applying it, than AC.

Unfortunately, we could only perform one set of measurements for each long fiber. Our results would certainly be more significant, if multiple measurements could have been taken. This would be one point of improvement for follow up experiments, next to the assurance of exact same environmental conditions throughout the whole experiment. This could be achieved with a light sensor inside the dark box.

One important aspect could not be covered in this project that is of great interest: How the different resins influence the lifetime of the fibers. Since the experimental design is repeatable, this can be done in the following months by repeating the same measurements for the long fibers.

Nevertheless, we obtained valuable insight in the properties of the resins. In conclusion, we can say that AC and EJ are both adequate for smaller prototypes, but in the real detector of T2K it is certainly recommendable to invest in the more expensive OF resin, as it loses less photons and can also be cured relatively quick using UV light.

## References

- [1] K. Abe et al. Constraint on the matter–antimatter symmetry-violating phase in neutrino oscillations. *Nature*, 580(7803):339–344, Apr 2020.
- [2] K. Abe et al. Measurement of neutrino and antineutrino oscillations by the t2k experiment including a new additional sample of  $\nu_e$  interactions at the far detector. *Phys. Rev. D*, 96:092006, Nov 2017.
- [3] K. Abe et al. Measurements of the t2k neutrino beam properties using the ingrid on-axis near detector. *Nuclear Instruments and Methods in Physics Research Section A: Accelerators, Spectrometers, Detectors and Associated Equipment*, 694:211–223, December 2012.
- [4] K. Abe et al. T2k nd280 upgrade – technical design report, 2020.
- [5] A. Blondel et al. A fully-active fine-grained detector with three readout views. *Journal of Instrumentation*, 13(02):P02006–P02006, February 2018.
- [6] The T2K Collaboration. About T2K. <https://t2k-experiment.org/t2k/>, [Accessed: June 2024].
- [7] Aoi Eguchi. The t2k near detector upgrade. *Physical Sciences Forum*, 8(1), 2023.
- [8] Lukas Gruber. LHCb SciFi - Upgrading LHCb with a scintillating fibre tracker. *Nuclear Instruments and Methods in Physics Research Section A: Accelerators, Spectrometers, Detectors and Associated Equipment*, 958:162025, 2020. Proceedings of the Vienna Conference on Instrumentation 2019.
- [9] Matthew Franks et al. Demonstration of particle tracking with scintillating fibres read out by a spad array sensor and application as a neutrino active target, 2023.
- [10] Eljen Technology. EJ-500 Optical Cement. <https://eljentechnology.com/products/accessories/ej-500> [Accessed: June 2024].
- [11] R. Mirabelli et al. The mondo detector prototype development and test: Steps toward an spad-cmos-based integrated readout (sbam sensor). *IEEE Transactions on Nuclear Science*, 65(2):744–751, 2018.

- [12] Kuraray. <https://www.kuraray.com/products/psf>, [Accessed: June 2024].
- [13] Hamamatsu Photonics. MPPC S13360/S13362 series. [https://www.hamamatsu.com/eu/en/product/optical-sensors/mppc/mppc\\_mppc-array.html](https://www.hamamatsu.com/eu/en/product/optical-sensors/mppc/mppc_mppc-array.html) [Accessed: June 2024].
- [14] Hamamatsu Photonics. MPPCs (SiPMs) / SPADs. <https://www.hamamatsu.com/eu/en/product/optical-sensors/mppc.html> [Accessed: June 2024].
- [15] CAEN Group. DT5202. <https://www.caen.it/products/dt5202/>, [Accessed: June 2024].
- [16] CAEN Group. JANUS FERS-5200 DAQ SOFTWARE. <https://www.caen.it/products/janus/>, [Accessed: June 2024].
- [17] AnyCubic. Colored UV Resin - Clear. <https://store.anycubic.com/products/colored-uv-resin?variant=34622234362018> [Accessed: June 2024].
- [18] MyPolymers. OF-133-V4: Optical Fiber Coating. <https://www.mypolymers.com/p/1925/> [Accessed: June 2024].
- [19] 3M. 3M Wetordry Sandpaper, 32035, 800 Grit. [https://www.3m.com/3M/en\\_US/p/d/v100010910/](https://www.3m.com/3M/en_US/p/d/v100010910/), [Accessed: June 2024].
- [20] Thorlabs. Fiber Polishing Supplies. [https://www.thorlabs.com/newgroupage9.cfm?objectgroup\\_id=1350](https://www.thorlabs.com/newgroupage9.cfm?objectgroup_id=1350).